



## Characterization of the nonlinear elastic properties of soft tissues using the supersonic shear imaging (SSI) technique: Inverse method, *ex vivo* and *in vivo* experiments

Yi Jiang <sup>a,1,2</sup>, Guo-Yang Li <sup>a,1</sup>, Lin-Xue Qian <sup>b,1</sup>, Xiang-Dong Hu <sup>b</sup>, Dong Liu <sup>b</sup>, Si Liang <sup>b</sup>, Yanping Cao <sup>a,\*</sup>

<sup>a</sup> Institute of Biomechanics and Medical Engineering, AML, Department of Engineering Mechanics, Tsinghua University, Beijing 100084, PR China

<sup>b</sup> Department of Ultrasound, Beijing Friendship Hospital, Capital Medical University, Beijing 100050, PR China



### ARTICLE INFO

#### Article history:

Received 18 February 2014

Received in revised form 15 August 2014

Accepted 31 October 2014

Available online 8 November 2014

#### Keywords:

Dynamic elastography

Supersonic shear imaging

Stressed hyperelastic soft tissues

*In vivo* experiments

Clinical diagnosis

### ABSTRACT

Dynamic elastography has become a new clinical tool in recent years to characterize the elastic properties of soft tissues *in vivo*, which are important for the disease diagnosis, e.g., the detection of breast and thyroid cancer and liver fibrosis. This paper investigates the supersonic shear imaging (SSI) method commercialized in recent years with the purpose to determine the nonlinear elastic properties based on this promising technique. Particularly, we explore the propagation of the shear wave induced by the acoustic radiation force in a stressed hyperelastic soft tissue described via the Demiray–Fung model. Based on the elastodynamics theory, an analytical solution correlating the wave speed with the hyperelastic parameters of soft tissues is first derived. Then an inverse approach is established to determine the hyperelastic parameters of biological soft tissues based on the measured wave speeds at different stretch ratios. The property of the inverse method, e.g., the existence, uniqueness and stability of the solution, has been investigated. Numerical experiments based on finite element simulations and the experiments conducted on the phantom and pig livers have been employed to validate the new method. Experiments performed on the human breast tissue and human heel fat pads have demonstrated the capability of the proposed method for measuring the *in vivo* nonlinear elastic properties of soft tissues. Generalization of the inverse analysis to other material models and the implication of the results reported here for clinical diagnosis have been discussed.

© 2014 Elsevier B.V. All rights reserved.

### 1. Introduction

Elastography which enables us to probe the elastic properties of living soft tissues has found wide medical applications during the past two decades (Ophir et al., 1991, 1999; Gao et al., 1996; Sandrin et al., 2002a,b; Bercoff et al., 2004; Doyley, 2012; Sarvazyan et al., 2011; Khaled and Ermert, 2008). The key steps behind the elastography are summarized in Fig. 1. First, an external or internal stimulus is imposed to a target soft tissue. Then the responses of the soft tissue including its deformation or the shear wave propagation in it are monitored by a medical imaging technique, e.g., the ultrasound or the nuclear magnetic resonance (NMR) imaging. The elastic or viscoelastic properties of the soft tissue may be inferred from the measured responses based on the

inverse analysis. It has been demonstrated that many diseases, e.g., cancer and the liver fibrosis, are usually accompanied by the variation of the tissue mechanical properties; therefore, the *in vivo* elastic properties of soft tissues given by the elastography are important for clinical diagnosis.

Fig. 1 demonstrates that continuum mechanics plays an essential role in both Steps (1) and (3). In Step (1), continuum mechanics is able to predict the responses of a biological soft tissue and so that an appropriate stimulus can be selected. For instance, in the quasi-static elastography pioneered by Ophir et al. (1991) and later developed by many others (e.g., Schaar et al., 2003; Miyanaga et al., 2006; Thitaikumar et al., 2007, 2008; Xu et al., 2011), a compressive load is usually imposed on the surface of a soft tissue; continuum mechanics predicts that the softer part will undergo greater deformation in comparison with the stiffer part. Therefore, measuring the deformation of the soft tissue using a medical imaging method enables us to differentiate the parts with different elastic modulus. In the transient elastography (Krouskop et al., 1987; Bercoff et al., 2004; Foucher et al., 2006; Gennisson et al., 2010; Rifai et al., 2011; Sarvazyan et al., 2013), the shear wave is usually

\* Corresponding author. Tel.: +86 10 62772520; fax: +86 10 62781284.

E-mail address: [caoyanping@tsinghua.edu.cn](mailto:caoyanping@tsinghua.edu.cn) (Y. Cao).

<sup>1</sup> These authors made equal contribution to this study.

<sup>2</sup> Present address: Beijing Institute of Astronautic Systems Engineering, Beijing 100076, PR China.

generated either using an external mechanical vibrator (e.g., Fibroscan, Echosens™) or by the acoustic radiation force (e.g., Supersonic Imagine, Aix-en-Provence, France). The analysis of the propagation of the shear wave in an elastic solid, which has long been a classical topic in continuum mechanics (Timoshenko and Goodier, 1951; Biot, 1940, 1965; Chadwick and Ogden, 1971; Ogden, 2007), allows one to evaluate the elastic properties of a soft tissue from the measured wave speed and its density. In Step (3), inferring the mechanical properties of a biological soft tissue from the responses of the soft tissue to an external or internal stimulus represents an inverse problem in elasticity. In comparison with the transient elastography, solving an inverse elastic problem corresponding to the quasi-static elastography may be more challenging because the deformation of the tested tissue depends on the loading and boundary conditions as well as its geometry. In this sense, a quantitative determination of the mechanical properties of a soft tissue using the quasi-static elastography usually represents a difficult issue (Mehravian et al., 2010; Gokhale et al., 2008; Pavan et al., 2012; Latorre-Ossa et al., 2012) and hence the transient elastography has received more and more attention in recent years. Currently, the widely used transient elastography instruments (e.g., Fibroscan and Supersonic Imagine) use a well-known formula developed for the shear wave propagating in a linear elastic solid to correlate the initial shear modulus  $\mu_0$  of a soft tissue with the wave speed  $c$  and the tissue density  $\rho$ , i.e.,

$$\mu_0 = \rho c^2. \quad (1)$$

Eq. (1) is very easy to use and welcome by the clinician; however, it may contain significant errors when the soft tissue undergoes finite deformation during a medical detection. Moreover, Eq. (1) does not enable us to determine the nonlinear elastic properties of a soft tissue. Based on this premise, this study is concerned with nonlinear mechanics behind the transient elastography; in particular, determining the nonlinear elastic properties of soft tissues using the supersonic shear imaging (SSI) technique (Bercoff et al., 2004) is investigated.

SSI is an ultrasound-based method, which uses the acoustic radiation force to stimulate two forceful plane shear waves in the target living tissue and measures the shear wave velocity through the recorded tissue displacement disturbed by the shear wave propagation. The merits and more details regarding this technique can be found in the classic paper of Bercoff et al. (2004). This technique has been commercialized and the software (Supersonic Imagine, Aix-en-Provence, France) uses Eq. (1) to compute the initial shear modulus from the wave velocity and the density of the soft tissue, which is a classical solution in the theory of linear elasticity. In a practical medical detection, Eq. (1) is not accurate any more when the deformation caused by the contact of the probe with the soft tissue (e.g., the breast and/or thyroid) is not small. In this case, the theory describing the shear wave propagating in

a deformed hyperelastic solid, which has been investigated by many authors in the mechanics community (Ogden, 1997, 2007; Hussain and Ogden, 2001; Holzapfel, 2000; Destrade et al., 2010), should be used. Recently, by including the effects of tissue deformation on the shear wave propagation, a number of authors have made efforts toward characterizing the nonlinear elastic properties of compliant materials or soft tissues using the SSI technique. For instance, Gennisson et al. (2007) have demonstrated the possibility to determine both the initial shear modulus and the third order elastic constants of a third-order solid. They measured the third-order elastic constants of the agar-gelatin and polyvinyl alcohol phantoms. Based on the same material model, Latorre-Ossa et al. (2012) proposed a method by combining the static elastography (Ophir et al., 1991) with the SSI technique to measure the third-order elastic constants. They validated their method by performing experiments on agar-gelatin phantoms and *ex vivo* beef livers. The above studies demonstrate that the SSI technique is promising in characterizing the hyperelastic properties of biological soft tissues which might be important for clinical diagnosis. However, the following fundamental issues involving both the theory and practical measurements require systematic investigations.

First, determining the hyperelastic parameters of a soft tissue using the SSI technique is an inverse problem. Therefore, it is necessary and important to suggest a general framework to develop inverse approaches to extract the nonlinear elastic properties of soft tissues from the experimental responses based on the current understanding on the propagation of the plane shear wave in a stressed hyperelastic solid and the mathematical theory of inverse problems.

Second, unlike direct problems, many inverse problems are ill-posed or ill-conditioned (Hadamard, 1923). Therefore, it is essential to explore the properties of the solution to the inverse problem, i.e., the existence, uniqueness and stability of the identified solution. This important issue has not been investigated in previous methods based on the SSI technique.

Third, experiments conducted in the literature (Latorre-Ossa et al., 2012; Gennisson et al., 2007) measured the hyperelastic parameters of some artificial materials, e.g., the agar-gelatin and polyvinyl alcohol phantoms, and the *ex vivo* nonlinear elastic constants of soft tissues using the SSI technique. To the authors' best knowledge, no effort has been made to measure the *in vivo* hyperelastic properties of a soft tissue using the SSI technique besides the initial shear modulus. In this sense, development of a robust method suitable for the *in vivo* measurement of the nonlinear elastic properties of soft tissues based on the SSI technique remains an important issue and deserves systematic investigation.

Bearing the above issues in mind, a comprehensive study combining theoretical analysis and numerical simulations with both the *ex vivo* and *in vivo* experiments is carried out in this paper. The paper is organized as follows: Section 2 gives the theory characterizing the propagation of the shear wave in a hyperelastic soft tissue described via the Demiray-Fung model. An analytical solution correlating the wave speed with the hyperelastic parameters of soft tissues and the stretch ratios is derived based on a general relation proposed by Ogden (2007). In Section 3, an inverse method is proposed to extract the hyperelastic properties of soft tissues from the SSI measurements. In Section 4, the stability of the identified solution using the proposed method is investigated. In particular, the condition number is derived in analytical form, which measures the sensitivity of the solution of the inverse problem to data errors. Numerical experiments are further performed to validate the novel inverse method. Experiments on the phantom and *ex vivo* experiments on pig livers are conducted in Section 5; the identified linear elastic and nonlinear elastic parameters are compared with the results given by the tensile and indentation tests and those reported in the literature to validate the proposed method in practical measurement. In Section 6, experiments are

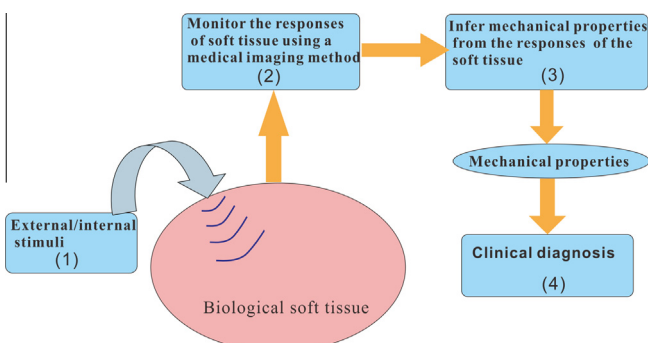


**Fig. 1.** An illustration of the key steps involved in the elastography.

performed on the human breast tissue and human heel fat pads. The results demonstrate the applicability of the proposed method to the measurement of *in vivo* nonlinear elastic properties of a soft tissue. Generalization of the direct and inverse analysis conducted in this study to other material models and the limitations in this study have been discussed in Section 7. Section 8 gives the concluding remarks.

## 2. Theoretical analysis on the propagation of the shear wave in a deformed hyperelastic solid

We consider the propagation of the shear wave induced by the acoustic radiation force in a deformed incompressible soft tissue as illustrated in Fig. 2. Fig. 2a shows the deformation caused by the contact of the probe with the soft tissue. Fig. 2b illustrates the shear waves induced by the acoustic radiation force along depth. In the SSI technique, the shear source travels along the depth at a supersonic speed, which is much faster than the traveling speed of the resulting shear waves. In theory, the generated shear waves interfere constructively along a 'Mach cone' (Bercoff et al., 2004). However, the Mach angle, which is proportional to the ratio between the shear wave speed and the traveling speed of the shear source, is rather small. Therefore, it is not explicitly shown in Fig. 2b. To address the effects of finite deformation and assess the nonlinear elastic properties, the theory describing the shear wave propagating in a stressed hyperelastic solid is invoked in this study to analyze how the wave velocity depends on the physical properties and deformation of a soft tissue. The key governing equations regarding the elastodynamics theory involved in this study are briefly introduced and more details can be found in Ogden (2007).

### 2.1. Governing equations in the involved elastodynamics theory

#### 2.1.1. Time-dependent deformation

A point in the reference configuration is labeled by the position vector  $\mathbf{X}$  and its position vector in the current configuration is  $\mathbf{x}$ , then the deformation gradient is given by

$$\mathbf{F} = \nabla \mathbf{x} = \frac{\partial \mathbf{x}}{\partial \mathbf{X}}, \quad (2)$$

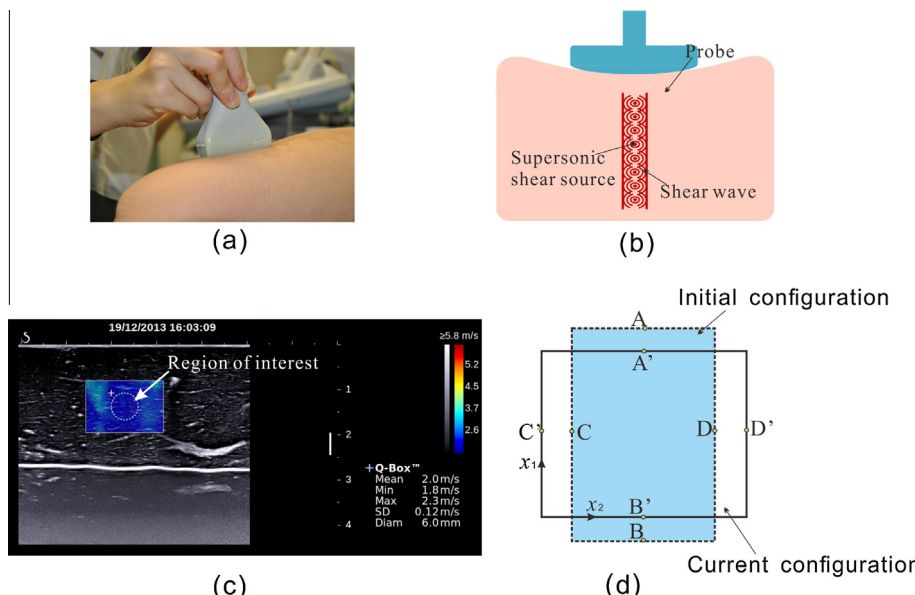


**Fig. 2.** Illustration of a practical measurement using the SSI technique. (a) Finite deformation may easily occur in a medical detection; (b) shear waves are generated in a deformed soft tissue by the acoustic radiation force; (c) the wave speeds in the region of interest can be measured using the instrument; and (d) schematic of the deformation state in the region of interest.

where  $\mathbf{X}$  and  $\mathbf{x}$  have the Cartesian coordinates  $X_i$  and  $x_i$ , respectively, with  $i, i \in \{1, 2, 3\}$ . " $\nabla$ " is the gradient operator. The velocity and acceleration of a material point are given by

$$\mathbf{v} \equiv \dot{\mathbf{x}}, \mathbf{a} \equiv \ddot{\mathbf{x}} \equiv \mathbf{x}_{tt}, \quad (3)$$

where  $t$  denotes time.  $\partial/\partial t$  and " $_{tt}$ " represent the material time derivative.

If the motion is isochoric then  $J = \det \mathbf{F} \equiv 1$ , in this case

$$\nabla \cdot \mathbf{v} = \frac{1}{J} \frac{\partial J}{\partial t} = 0, \quad (4)$$

where " $\nabla \cdot$ " represents the divergence operator related to the current configuration.

#### 2.1.2. Motion equations

The motion equation may be written as

$$\nabla_0 \cdot \mathbf{S} = \rho \mathbf{a}, \quad (5)$$

where " $\nabla_0 \cdot$ " represents the divergence operator in the reference configuration,  $\rho$  is the mass density, which is constant for an incompressible material. The nominal stress tensor  $\mathbf{S}$  is related to the strain energy function  $W$  by

$$\mathbf{S} = \frac{\partial W}{\partial \mathbf{F}} - p \mathbf{F}^{-1}, \quad (6)$$

where  $p$  is the Lagrange multiplier associated with the incompressibility constraint. Inserting Eq. (6) into (5) gives

$$\Xi_{ijj} x_{i,jj} - p_{,i} = \rho x_{i,tt}, \quad (7)$$

where

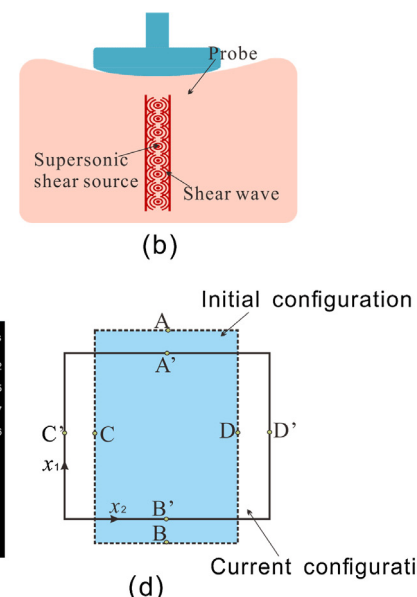
$$\Xi_{ijj} = \Xi_{jjj} = \frac{\partial^2 W}{\partial F_{ii} \partial F_{jj}}. \quad (8)$$

The Einstein's summation convention for repeated indices is adopted here and in the sequel.  $F_{ij}$  represent the components of the deformation gradient tensor.

#### 2.1.3. Incremental motion equations

The incremental displacement can be expressed as

$$\mathbf{u}(\mathbf{x}, t) = \dot{\mathbf{x}}, \quad (9)$$



where the superposed dot represents an increment. The incremental motion equation may be expressed as

$$\nabla_0 \cdot \dot{\mathbf{S}} = \rho \dot{\mathbf{x}}_{tt}. \quad (10)$$

For an incompressible material, the incremental nominal stress can be written as  $\dot{\mathbf{S}} = \Xi \dot{\mathbf{F}} - \dot{p} \mathbf{F}^{-1} + p \mathbf{F}^{-1} \dot{\mathbf{F}} \mathbf{F}^{-1}$  (Ogden, 2007). In many cases, it is convenient to use the motion equation in the deformed configuration. The incremental stress in deformed configuration is related to  $\dot{\mathbf{S}}$  by

$$\dot{\boldsymbol{\sigma}} = J^{-1} \mathbf{F} \dot{\mathbf{S}}, \quad (11)$$

then the incremental motion equation in deformed configuration is given by

$$\nabla \cdot \dot{\boldsymbol{\sigma}} = \rho \dot{\mathbf{x}}_{tt}. \quad (12)$$

The incompressible condition reads

$$tr(\dot{\mathbf{F}} \mathbf{F}^{-1}) = u_{ii} = 0, \quad (13)$$

where “*tr*” denotes the trace of a tensor.

## 2.2. Shear wave propagation in a stressed hyperelastic solid described with the Demiray–Fung model

In a practical medical detection using the SSI technique as shown in Fig. 2c, a region of interest will be selected in which the average value for the shear wave speed is provided. The strain field caused by the contact of the probe with the soft tissue generally is not homogeneous. However, when strain gradient in the region of interest (Fig. 2c) is small, it is rather reasonable to assume that in this region the principal stretch ratios  $\lambda_1, \lambda_2, \lambda_3$  along loading direction and the perpendicular directions (Fig. 2d) are homogeneous, i.e., they are independent of  $X_I$  ( $I = 1, 2, 3$ ). The deformation state shown in Fig. 2d can be described by the equations

$$x_1 = \lambda_1 X_1, \quad x_2 = \lambda_2 X_2, \quad x_3 = \lambda_3 X_3, \quad (14a)$$

$$F_{ij} = \begin{bmatrix} \lambda_1 & & \\ & \lambda_2 & \\ & & \lambda_3 \end{bmatrix}. \quad (14b)$$

For an incompressible hyperelastic material,

$$\lambda_1 \lambda_2 \lambda_3 = 1. \quad (15)$$

When deformation in the region of interest is homogeneous, Eqs. (11) and (12) give

$$\Xi_{0kij} u_{j,kl} - \dot{p}_{,i} = \rho u_{i,tt}, \quad (16)$$

where

$$\Xi_{0kij} = J^{-1} F_{kl} F_{ij} \Xi_{lij}. \quad (17)$$

We here focus on the propagation of the plane shear wave generated by the acoustic radiation force in a stressed soft tissue with the deformation state given by Fig. 2d. The plane shear wave may be written in the following form

$$\Phi = A \exp[ik(x_1 \cos \vartheta + x_2 \sin \vartheta - ct)], \quad (18)$$

where  $k$  is the wave number,  $\vartheta$  is the angle between the loading direction and the propagation direction of the wave.  $A$  is the amplitude and  $c$  the wave speed. The plane incremental displacement components can be expressed as

$$u_1(x_1, x_2, 0), \quad u_2(x_1, x_2, 0), \quad u_3 = 0, \quad (19)$$

and based on Eq. (13) they are related to  $\Phi$  by

$$u_1 = \Phi_{,2}, \quad u_2 = -\Phi_{,1}. \quad (20)$$

Eqs. (16), (18) and (20) enable us to obtain an analytical solution relating the wave speed to the material properties and the deformation state. This issue has been solved in previous studies (Ogden, 2007) and a general solution in the following form proposed

$$(\alpha + \gamma - 2\beta) \cos^4 \vartheta + 2(\beta - \gamma) \cos^2 \vartheta + \gamma = \rho c^2, \quad (21)$$

where

$$\alpha = \Xi_{01212}, \quad 2\beta = \Xi_{01111} + \Xi_{02222} - 2\Xi_{01122} - 2\Xi_{01221}, \quad \gamma = \Xi_{02121}. \quad (22)$$

Eq. (21) holds true for both isotropic and anisotropic hyperelastic materials. In our present issue,  $\vartheta = 90^\circ$ , and Eq. (21) reduces to

$$\rho c^2 = \gamma = \Xi_{02121}. \quad (23)$$

When both the constitutive law defined by the strain energy function and the deformation state are specified, Eq. (23) can give the correlation between the material parameters and the wave speed.

The soft tissue interested here is assumed to be isotropic and quasi-incompressible and described with the following strain energy function (Demiray, 1972; Fung et al., 1979; Fung, 1993)

$$W = \frac{\mu_0}{2b} (e^{b(I_1 - 3)} - 1), \quad (24)$$

where  $\mu_0$  and  $b$  are material parameters;  $\mu_0$  represents the initial shear modulus and  $b$  defines the hardening behavior.  $I_1 = \lambda_1^2 + \lambda_2^2 + \lambda_3^2$ . Eq. (24) is written in terms of  $\lambda_i$  and then related to the deformation state defined by Eq. (14). Let  $\lambda_1 = \lambda$  and  $\lambda_2 = \lambda_1^{-\xi}$ , from Eq. (15) we have  $\lambda_3 = \lambda^{-(1-\xi)}$ , where  $\xi$  is a parameter. For the deformation state concerned in this study and illustrated in Fig. 2d,  $\xi$  is in the range of 0–1. It can be easily found that  $\xi = 1$  or  $\xi = 0$  represents a plane strain compression and  $\xi = 0.5$  a uniaxial compression.

Eqs. (17) and (14) give  $\Xi_{02121} = \lambda_2^2 \Xi_{2121} = \lambda^{-2\xi} \Xi_{2121}$ , and from Eqs. (8) and (14b), we have  $\Xi_{2121} = 2 \frac{\partial W}{\partial I_1}$ . These two relations together with Eq. (24) give

$$\Xi_{02121} = \mu_0 \lambda^{-2\xi} e^{b(\lambda^2 + \lambda^{-2\xi} + \lambda^{-2(1-\xi)} - 3)}. \quad (25)$$

Eqs. (23) and (25) stand

$$\rho c^2 = \mu_0 \lambda^{-2\xi} e^{b(\lambda^2 + \lambda^{-2\xi} + \lambda^{-2(1-\xi)} - 3)}. \quad (26)$$

Eq. (26) is the fundamental solution obtained in this study upon which an inverse approach will be established to extract the hyperelastic properties of a soft tissue. For the shear wave propagating in a stress-free solid, i.e.,  $\lambda = 1$ , Eq. (26) degenerates to the classical solution of  $\rho c^2 = \mu_0$ . To reveal the role played by the parameter  $\xi$ , we plot in Fig. 3 the variation of the wave speed with  $\xi$  for different  $\lambda$ .

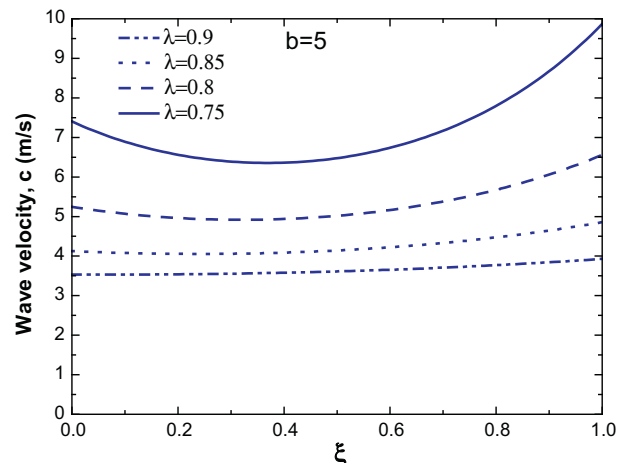


Fig. 3. Dependence of the wave speed on the parameter  $\xi$  for different  $\lambda$ .

$\lambda$  by taking  $b = 5$  as an example. It can be seen from the figure that  $\xi$  has negligible effects on the wave speed when the deformation is relatively small (e.g.,  $\lambda = 0.9$ ). Actually, when  $0.1 \leq \xi \leq 0.8$ , its influence on the wave velocity is not significant. Therefore, in this case it is reasonable to take  $\xi$  as a fixed value, e.g.,  $\xi = 0.3$ . However, difference between the uniaxial compression ( $\xi = 0.5$ ) and the plane strain compression ( $\xi = 1$ ) is pronounced when the compressive amount is large, e.g.,  $\lambda = 0.75$ . In this sense, it is suggested to evaluate  $\xi$  besides the determination of  $\lambda$ . In the next section, we provide a means to evaluate  $\lambda$  and  $\xi$  in a practical measurement.

### 3. An inverse method to determine the hyperelastic properties of soft tissues using the SSI technique

The analytical solution given by Eq. (26) enables us to develop an inverse approach to determine the hyperelastic properties of a soft tissue using the SSI technique. Eq. (26) indicates that when the deformation of the soft tissue is negligible, i.e.,  $\lambda \approx 1$ , the initial shear modulus  $\mu_0$  can be determined from the measured wave speed and the mass density. This has been realized in the commercialized SSI technique. Eq. (26) also demonstrates the possibility to determine the hyperelastic parameter  $b$ , which defines the nonlinearity of the soft tissue. With the known  $\mu_0$  and the measured  $c$  at different  $\lambda$ , the parameter  $b$  can be determined from Eq. (26) with

$$b = \frac{\ln\left(\frac{\rho c^2 \lambda^{2\xi}}{\mu_0}\right)}{\left(\lambda^2 + \lambda^{-2\xi} + \lambda^{-2(1-\xi)} - 3\right)}. \quad (27)$$

Eq. (27) is in analytical form, thus it is very convenient for practical use. It should be pointed out that the parameters  $\lambda$  and  $\xi$  should be determined besides the wave speed  $c$  in the use of Eq. (27). To this

end, a simple means is to evaluate the displacements at four points as illustrated in Fig. 2d. In a practical measurement, four characteristic points in the region of interest, e.g., A, B, C and D in Fig. 2d, can be selected. In the deformed configuration, they are A', B', C' and D', respectively. From the ultrasound image, the distance between A and B and that between C and D are denoted as  $l_{AB}$  and  $l_{CD}$ , respectively. In the deformed configuration, the distance between A' and B' and that between C' and D' can also be measured and denoted as  $l_{A'B'}$  and  $l_{C'D'}$ , respectively. The ratio of  $l_{A'B'}/l_{AB}$  gives  $\lambda$ ; and the ratio of  $l_{C'D'}/l_{CD}$  and  $\lambda$  give the parameter  $\xi$ . It is worth mentioning that in previous studies, the uniaxial loading condition ( $\xi = 0.5$ ) has been assumed in the determination of the nonlinear elastic parameters of a soft tissue using the SSI technique. This loading condition is not easy to achieve in an *in vivo* measurement. In this sense, introducing the parameter  $\xi$  on one hand permits to describe the deformation state more accurately and on the other hand enables us to evaluate the extent to which the assumption of the uniaxial loading is acceptable in an *in vivo* measurement.

### 4. Theoretical and numerical validations of the inverse method

#### 4.1. Theoretical analysis on sensitivity of the identified solution to data errors

Determining the hyperelastic parameters of a soft tissue using the SSI technique and Eq. (27) represents an inverse problem. Unlike direct problems, many inverse problems are ill-posed (Hadamarad, 1923). When the input data is polluted by the noises/errors, the identified solution to an ill-posed problem may have nothing to do with the true solution. Therefore, it is necessary and important to explore the properties of the solution to the

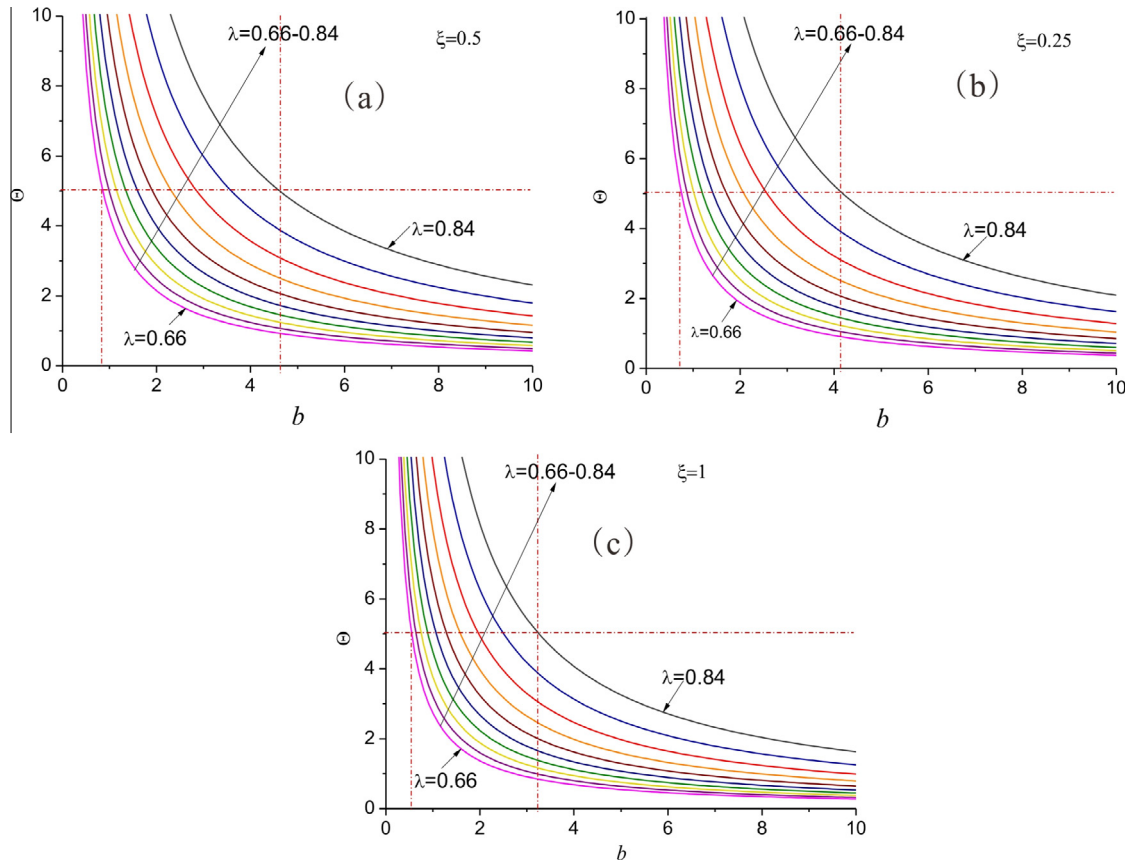
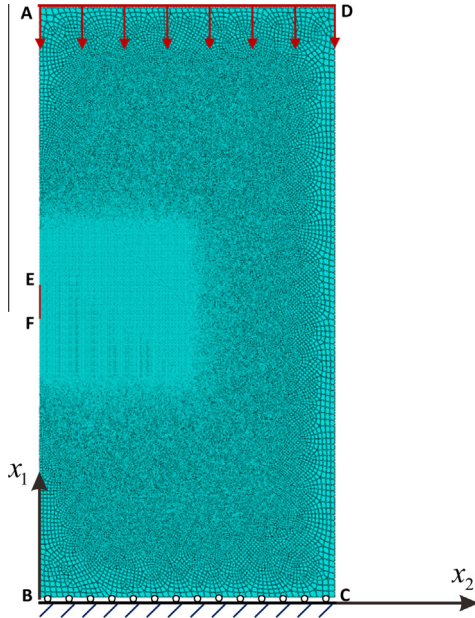


Fig. 4. Dependence of the condition numbers on the parameters  $\lambda$  and  $b$ . (a)  $\xi = 0.5$ ; (b)  $\xi = 0.25$ ; and (c)  $\xi = 1$ .

inverse problem, i.e., the existence, uniqueness and stability of the identified solution. From Eq. (27) it can be easily found the existence and uniqueness of the solution to the present inverse problem can be guaranteed. Therefore, here we focus on the stability issue, i.e., the sensitivity of the identified solution to the data errors. Particularly, we derive the condition number in a closed-form which measures the sensitivity of the identified hyperelastic parameters to the errors in the measured wave speeds. The initial shear modulus is determined using the equation of  $\rho c^2 = \mu_0$ , i.e.,  $\mu_0$  scales with the  $c^2$ . Therefore the condition number for the determination of  $\mu_0$  is 2. This indicates that 2% error in the measured  $c$  may lead to 4% error in the identified  $\mu_0$ . The condition number, which measures the sensitivity of the identified  $b$  to the errors in the measured  $c$ , is derived based on Eq. (27) as

$$\Theta = \frac{c}{b} \frac{\Delta b}{\Delta c} = \frac{2}{b(\lambda^2 + \lambda^{-2\xi} + \lambda^{-2(1-\xi)} - 3)}. \quad (28)$$



**Fig. 5.** Finite element model used in our simulations.

We plot the condition number given by Eq. (28) for different  $\lambda$  and  $b$  in Fig. 4. The results in this figure provide insight into the solution to the present inverse problem and provide guidelines for the experimental set-up. For instance, from the figure it can be seen that the smaller the parameter  $\lambda$ , the more reliable the identified  $b$ . Taking  $\Theta = 5$  as a critical value, at which a 2% error in the measured  $c$  may lead to 10% error in the identified  $b$ , Fig. 4a shows that the parameter  $b$  within the range of  $b \geq 0.8$  may be identified if the data for  $\lambda = 0.66$  is used; however, if the data corresponding to  $\lambda = 0.84$  is adopted in the inverse analysis, the identified parameter  $b$  may be reliable only when it is greater than 4.5. The numerical experiments will be performed in the next section to confirm the findings revealed by the theoretical analysis conducted here.

#### 4.2. Numerical experiments to validate the inverse method

Numerical experiments are performed in this paper to validate the reliability of the identified solution given by Eq. (27). In order to simulate the process of SSI and acquire the shear wave velocity at different compressive strains, a finite element simulation is carried out in this section using the commercial software – **ABAQUS** (2010). We implanted the constitutive model given by Eq. (24) into ABAQUS via the user subroutine **UHYPER**. A plane-stress model has been built to simulate the propagation of the shear wave in a uniaxial compressed hyperelastic solid. The model shown in Fig. 5 consists of 128 164 eight-node reduced integration plane-stress elements.

Along the edge BC in Fig. 5, the displacement in  $x_1$  direction is set to be zero with the traction free in the  $x_2$  direction. Uniaxial compression is imposed along the edge AD, with the stretch ratio  $\lambda$  varying from 1 to 0.7, which can be easily achieved in the test of most soft materials. To stimulate the plane shear wave propagating along  $x_2$  direction, a distributed shear load in the form of  $T = T_0 \sin \zeta t$  is imposed to the EF region in the model at different given stretch ratios  $\lambda$ , where  $T_0$  is the amplitude of the shear load,  $\zeta$  is the frequency and  $t$  the time. The finite element simulations give the wave length  $l_s$ , as shown in Fig. 6. In our simulations,  $T_0$  is much smaller than the initial shear modulus of the material and the amplitude of the generated shear wave is much smaller than the wave length  $l_s$ . The wave speed is computed using the relation of  $c = \zeta l_s$ .

The wave speeds at different compressive strains are used as the inputs of Eq. (27) to identify the parameter  $b$ . The identified

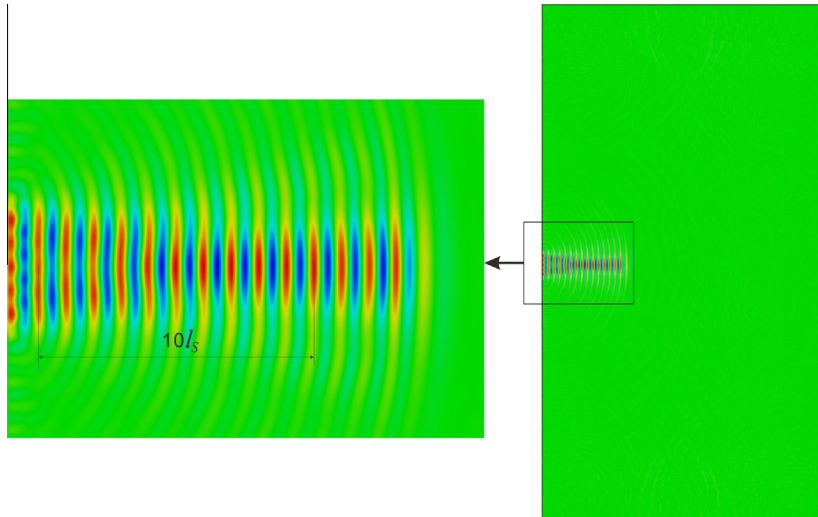


**Fig. 6.** Propagation of the plane shear wave in a hyperelastic solid with  $b = 4$  and  $\lambda = 0.95$ . The average wave length for ten waves is taken as  $l_s$ .

**Table 1**

A comparison of the identified  $b$  at different stretch ratios  $\lambda$  with the parameter  $b$  inputted in the simulations. In our simulations, we take  $b = 2, 4, 6$ , respectively, by referring to the possible values for pig livers.

$\lambda$	$c$ (Eq. (26)) (m/s)	$c$ (FEM) (m/s)	Identified $b$
$b = 2$			
0.95	3.27	3.20	−3.55
0.9	3.44	3.37	0.68
0.85	3.70	3.64	1.59
0.8	4.07	4.02	1.84
0.75	4.59	4.52	1.86
$b = 4$			
0.95	3.30	3.23	−0.91
0.9	3.56	3.51	3.13
0.85	3.99	3.94	3.65
0.8	4.68	4.59	3.73
0.75	5.77	5.68	3.85
$b = 6$			
0.95	3.32	3.27	1.71
0.9	3.67	3.62	5.19
0.85	4.30	4.25	5.66
0.8	5.38	5.29	5.74
0.75	7.26	7.10	5.80

$b$  and the actual solution are given in Table 1 for different  $\lambda$ . The actual solution here represents the parameter which is inputted in the finite element simulations. From Table 1 it can be seen that the computed wave speeds match the theoretical solutions well. However, when the stretch ratio  $\lambda$  is large (i.e., the compressive strain is small), the identified  $b$  from the inverse analysis is very sensitive to data errors. This finding is consistent with the theoretical predictions in Section 4.1. Therefore, in order to get a reliable  $b$ , it is suggested to use the data at relatively small stretch ratios  $\lambda$ . Besides, in a practical measurement, the parameter  $b$  at different  $\lambda$  can be determined using Eq. (27) and the average value taken as the final result.

## 5. Experiments performed on the phantom and pig livers to validate inverse method

### 5.1. Experiments on the phantom to validate the inverse method

In this section, we performed experiments on the phantom to verify the proposed method. A homogeneous tissue-mimicking phantom was made from polyvinyl alcohol powder (PVA) solution. The solution had 87% by weight of degassed distilled water, 10% of PVA (Sigma-Aldrich, Shanghai, China) and 3% of Sigmacell with particle diameter of about 20  $\mu\text{m}$  (Sigma-Aldrich, Shanghai, China), which acted as scattering particles. The solution container was heated in hot water to about 85 °C and stirred until it was fully dissolved. Thereafter, it was poured into a metal mold. The mold containing the solution was stored in a freezer (−20 °C) for 12 h and then thawed in room temperature (20 °C) for 12 h. Tensile tests were conducted to characterize the initial shear modulus  $\mu_0$  and the nonlinear elastic parameter  $b$  of the phantom. Considering that the initial part of the tensile curve might be polluted by the errors, which could affect the determination of  $\mu_0$ , indentation tests were further conducted in this paper to evaluate  $\mu_0$ . Both tensile and indentation tests were carried out using the ElectroForce® 3100 test instrument (Bose, Fig. 7). The force transducer can reach a maximum load of 2.5 N. The displacement resolution is 1  $\mu\text{m}$  and the load resolution is 0.1 mN. A spherical indenter made of stainless steel with a tip radius of  $R = 3 \text{ mm}$  was adopted in indentation tests. Displacement controlled loading procedure was applied. Four tensile tests were conducted and the indentation tests were performed on five different positions of the specimen. Fig. 8a showed the average tensile curve together with the error bar representing the standard deviation. Fitting the tensile curve using the

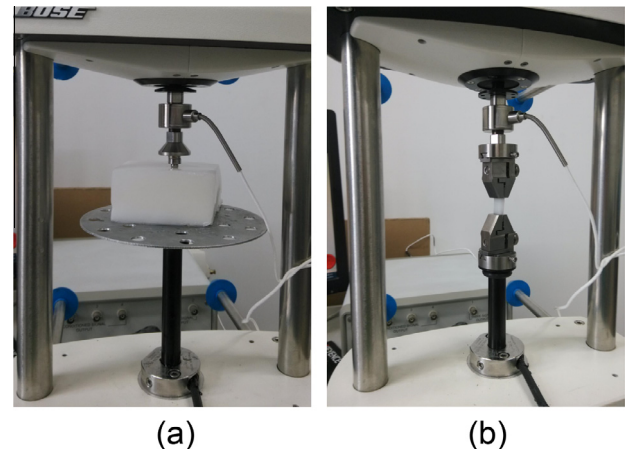


**Fig. 7.** Indentation (a) and tensile tests (b) performed using the ElectroForce® 3100 (Bose). The specimen used in the indentation tests has a width of 80 mm, a length of 80 mm and a thickness of 35 mm. The maximum indentation depth is 2 mm in our tests and in this case the effect of the substrate is negligible.

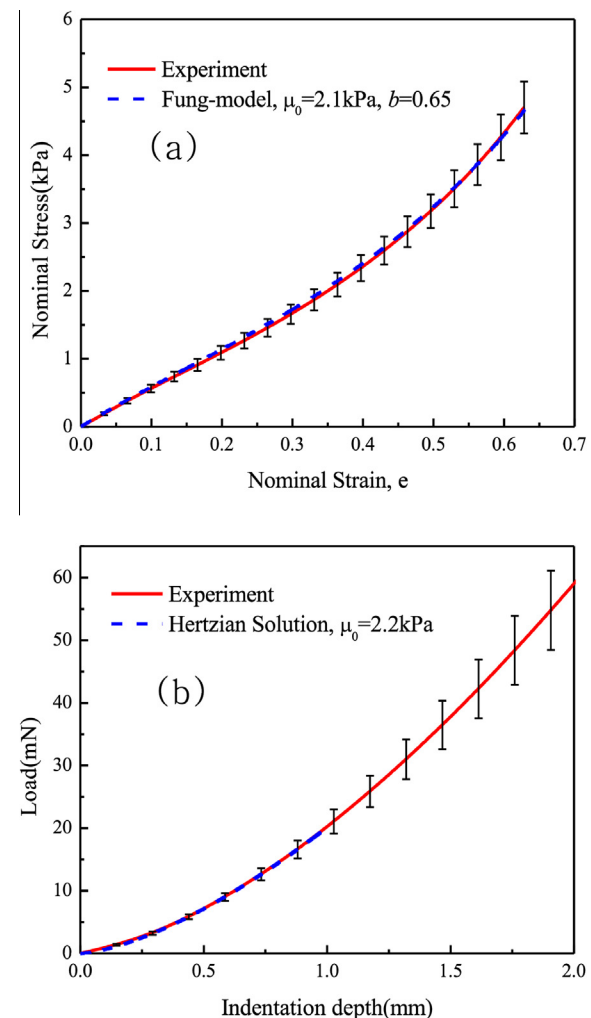


**Fig. 8.** Plots of the average tensile curve (a) and the indentation loading curve (b). The error bars in the figure represent the standard deviations. The analytical solution of  $S_1 = \mu_0 e^{b(\lambda^2 + 2\lambda^{-1} - 3)} (\lambda - \lambda^{-2})$  was used to fit the tensile curve to evaluate  $\mu_0$  and  $b$ . The Hertzian solution of  $p = \frac{16}{3} \mu_0 \sqrt{R} h$  was adopted to fit the initial part of the indentation loading to determine  $\mu_0$ , where  $p$  and  $h$  are the indentation load and indentation depth, respectively.

analytical solution of  $S_1 = \mu_0 e^{b(\lambda^2 + 2\lambda^{-1} - 3)} (\lambda - \lambda^{-2})$  for the Demiray-Fung model, we got  $\mu_0 = 2.1 \pm 0.1$  kPa and the parameter  $b = 0.65 \pm 0.1$ , where  $S_1$  is the nominal stress. Fig. 8b gave the average indentation loading curve. Fitting the initial part of the indentation loading curve using the Hertzian solution gave the initial shear modulus  $\mu_0 = 2.2 \pm 0.2$  kPa, which matched the value from the tensile tests well.

We then used the proposed method and the SSI technique to characterize the elastic properties of the phantom. The same specimen as used in indentation tests was adopted. The Aixplorer® ultrasound instrument (Supersonic Imagine, Aix-en-Provence, France) was used to measure the shear wave speeds in both the stress-free and deformed sample, upon which the SSI technique has been implemented.

The experimental procedure is described as follows:

- (1) The probe was first put vertically on the surface of the sample. The probe has no contact with the specimen, which was put in the water. Using the SSI technique, we measure the shear wave speed and so that the initial shear modulus  $\mu_0$  in the region of interest (the circled region in Fig. 9). The characteristic points in the image (Fig. 9) were used to determine the distances  $l_{AB}$  and  $l_{CD}$  as described in Fig. 2. The characteristic point A is a point at the upper boundary of the specimen. The characteristic points B(C) and D were generated by inserting two copper fibers with a diameter of 135  $\mu$ m into the specimen.
- (2) Then the compression was imposed by indenting the probe vertically to the surface. At a given indentation depth, the wave speed was measured. The characteristic points now moved to the new positions.  $l_{A'B'}$  was measured and then  $\lambda$  was determined.  $\xi$  was taken as 0.2 according to the variation of  $l_{CD}$  during the loading procedure.
- (3) Increasing the indentation depth by moving the probe down, the procedure in Step (2) is repeated to measure the corresponding wave speeds for different  $\lambda$ .

Fig. 10 showed the variation of the wave speeds with the compressive amount for two independent measurements. From the first test with the results gave by Fig. 10(a) and Eq. (26), we got

$\mu_0 = 2.4 \pm 0.15$  kPa, and  $b = 0.6 \pm 0.05$ . From the second test with the results given in Fig. 10(b), we obtained  $\mu_0 = 2.5 \pm 0.2$  kPa and  $b = 0.56 \pm 0.04$  using the inverse method proposed in Section 3. The initial shear modulus matches those given by the tensile and indentation tests well. The nonlinear elastic parameter  $b$  is close to the value obtained from our tensile tests. This indicates that the inverse method proposed in this paper is promising for characterizing the hyperelastic properties of soft materials.

## 5.2. Ex vivo experiments on pig livers to validate the inverse method

We further carried out ex vivo experiments on three pig livers to testify the applicability of the proposed method to the characterization of nonlinear elastic properties of soft tissues. The Aixplorer® ultrasound instrument (Supersonic Imagine, Aix-en-Provence, France) was used in the measurements. The details regarding the materials, measurements and results are described in detail below.

### 5.2.1. Materials

The porcine livers as shown in Fig. 11 obtained from three freshly slaughtered animals were used in our experiments. The fresh porcine livers were kept between 2 °C and 4 °C in an ice box and transported to the Beijing Friendship Hospital within 12 h postmortem, where the measurements were carried out.

### 5.2.2. Measurements

Measurements were performed at room temperature, and the humidity is around 50%. The Aixplorer transducer of SL15-4 was adopted in our experiments.

The experimental procedure described in Section 5.1 is basically followed in the measurements. Fig. 12 gives the wave speeds recorded by the Supersonic Imagine at two different contact depths for the pig #2. It can be clearly seen from the figure that the wave speed increases with the increase in the compressive amount.

### 5.2.3. Results and analysis

The initial shear moduli given by the SSI technique for the livers from three pigs are 3.5 kPa, 3.2 kPa and 3.7 kPa for Pigs #1, #2, and #3, respectively. These results appear to be smaller than those

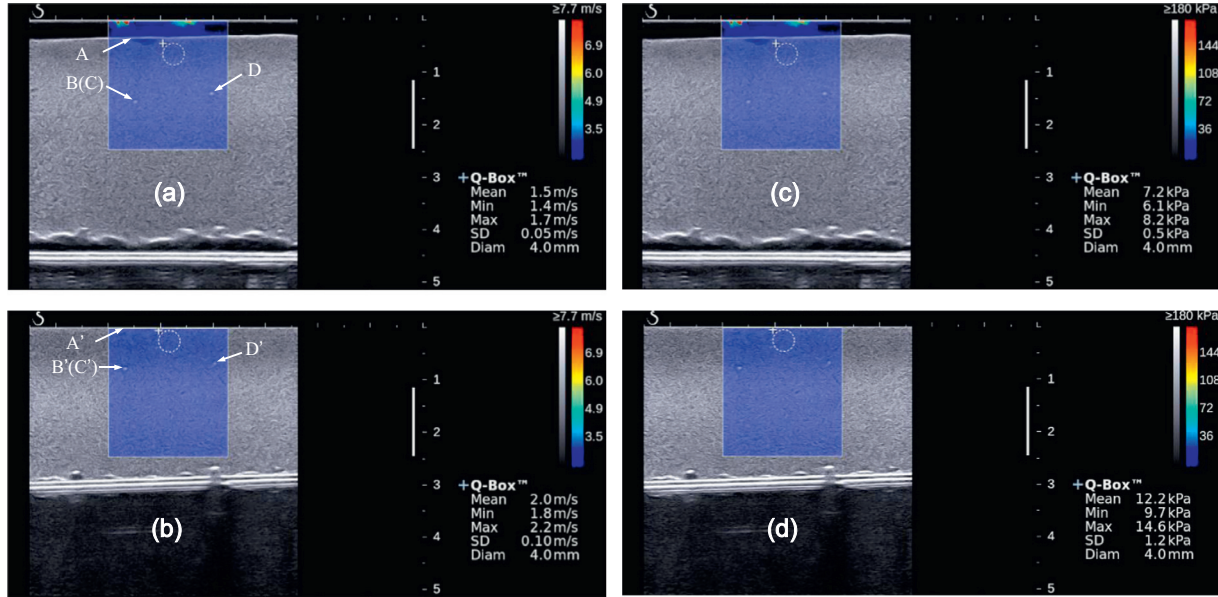
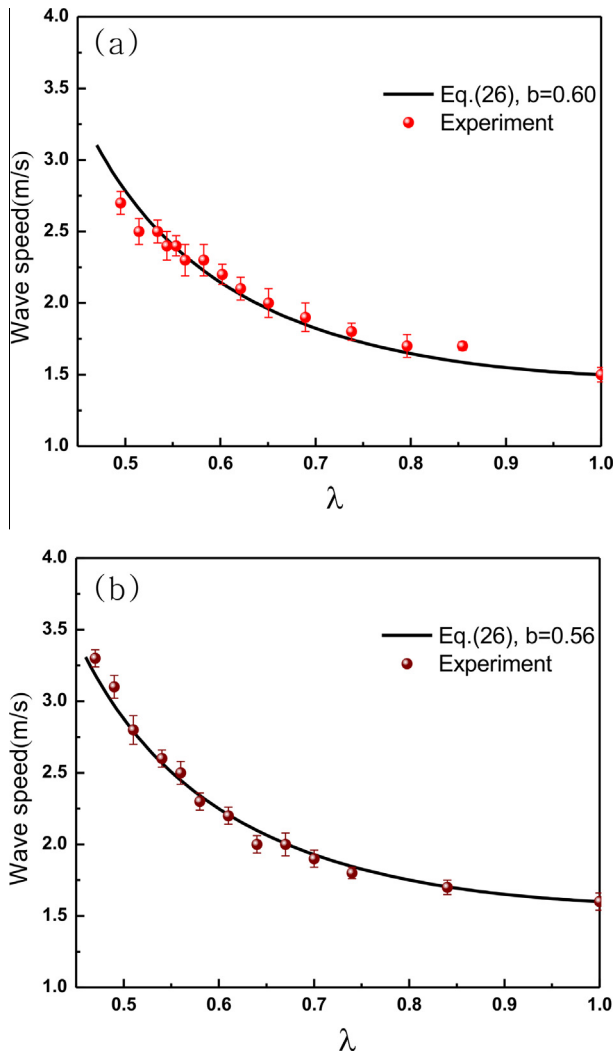
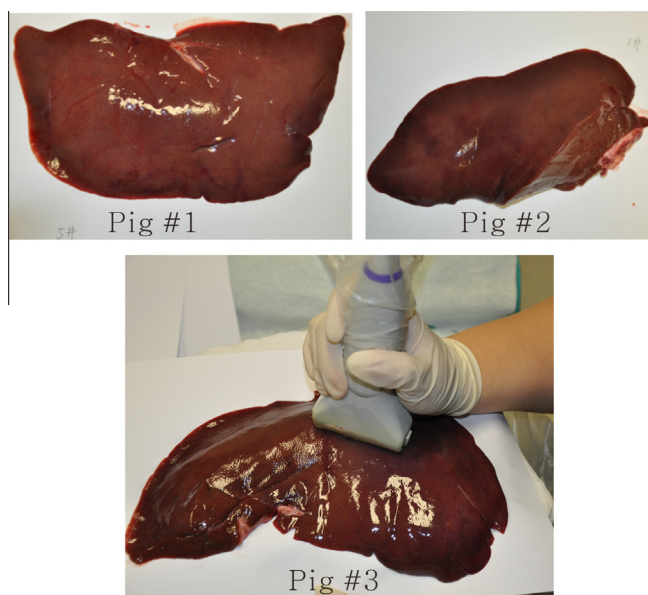


Fig. 9. Wave speeds and the elastic moduli in the region of interest (circled region in the figure) at two different indentation depths. (a) wave speeds in the stress-free sample; (b) wave speeds in the deformed sample; (c) elastic moduli in the stress-free sample; and (d) elastic moduli in the deformed sample.



**Fig. 10.** Variation of the wave speeds with the stretch ratio  $\lambda$  for two independent measurements. Points represent experimental results and lines are the predicted solutions using Eq. (26).



**Fig. 11.** Porcine livers from three different animals.

given by the indentation and pipette aspiration tests (Zhang et al., 2014). This may be attributed to the effect of the capsule layer, which does not come into play in the SSI measurement performed here but plays a role in both indentation and pipette aspiration tests. The measured wave speeds  $c$  at different  $\lambda$  are plotted in Fig. 13, which together with (27) enable us to evaluate the hyperelastic parameter  $b$ . The values of the parameter  $b$  are  $3.1 \pm 0.4$ ,  $3.7 \pm 0.3$  and  $4.7 \pm 0.5$  for pigs # 1, # 2, and #3, respectively. For each subject, the parameter  $b$  can be determined using the data at different  $\lambda$ . The variations of  $b$  as shown above demonstrate a relatively good reproducibility. Roan and Vemaganti (2007) characterized the nonlinear elastic properties of porcine livers by applying their analysis method to the uniaxial compression data of Chui et al. (2004). The parameter  $b$  obtained in their study was about 2.96. Compared with the result reported in their study, the values obtained here are in reasonable range, indicating that the new method is applicable for characterizing the hyperelastic properties of soft tissues.

## 6. Applications of the inverse method to measuring the *in vivo* nonlinear elastic properties of human soft tissues

All the measurements involved in the present inverse method can be carried out with the commercialized instrument-Supersonic Imagine. Therefore, the method proposed here is suitable for characterizing the *in vivo* nonlinear elastic properties of soft tissues. To demonstrate this point, we measure the *in vivo* hyperelastic parameters of the human breast tissue and the human heel fat pads. The measurements were performed at room temperature, and the humidity is around 50%.

### 6.1. Human breast tissue

Determination of the elastic properties of the human breast tissue is of great importance for some disease diagnosis, e.g., detection of the adenocarcinoma. Here we demonstrate the applicability of the proposed inverse method to the measurement of the *in vivo* nonlinear elastic properties of breast tissues. The procedures described in Section 5 were followed in the *in vivo* tests. A volunteer of 23 years old lay on her back and the measurement was performed on the upper-left part of the breast. By indenting the probe slowly, we measured the shear wave speeds at different contact depths in the glandular tissue of the breast, where some diseases, e.g., the adenocarcinomas, always occur. Fig. 14 shows the wave speeds in the region of interest at two different indentation depths.

In our experiments, the initial shear modulus  $\mu_0$  of the glandular tissue given by the SSI measurement is around 2 kPa, which corresponds to an elastic modulus of 6 kPa. In the literature (Gefen and Dilman, 2007), the elastic modulus of the glandular tissue is reported in range of 2–66 kPa depending on the testing methods. Based on the wave speeds corresponding to  $\lambda \leq 0.85$ , the hyperelastic parameter  $b$  is determined using Eq. (27), which is  $b = 3.0 \pm 0.4$  as given in Fig. 15. The nonlinear elastic parameter  $b$  may have significance in the use of the elastography to differentiate benign from malignant breast lesions. For instance, a proper compression is important in a measurement based on quasi-static elastography (Itoh et al., 2006; Burnside et al., 2007) to detect the property of a breast lesion. On one hand, the compression should be sufficient to induce deformation in the breast tissue; on the other hand, an over high compression may lead to hardening especially in the tissue around the lesions (Itoh et al., 2006). In this sense, the knowledge on the nonlinear elastic parameter of the glandular tissue may help determine the appropriate compressive amount in a clinical detection. Besides, the parameter  $b$  together with Eq. (26) enables us to quantitatively assess the extent to

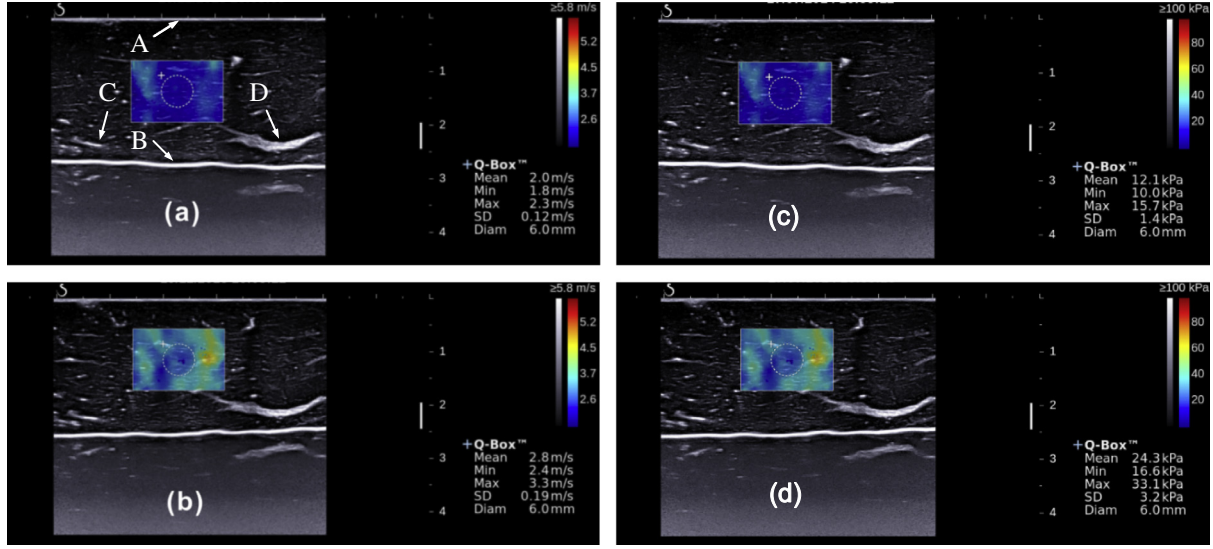


**Fig. 12.** Wave speeds and the elastic moduli in the region of interest (circled region in the figure). (a) wave speeds at  $\lambda = 0.87$ ; (b) wave speeds at  $\lambda = 0.77$ ; (c) elastic moduli at  $\lambda = 0.87$ ; (d) elastic moduli at  $\lambda = 0.77$ . The characteristic points A and B are used to determine  $\lambda$ ,  $\xi$  is in the range of 0.1–0.3. Fig. 3 shows that the effect of  $\xi$  does not change significantly when it varies in this range and it is taken as 0.2 in the data analysis.

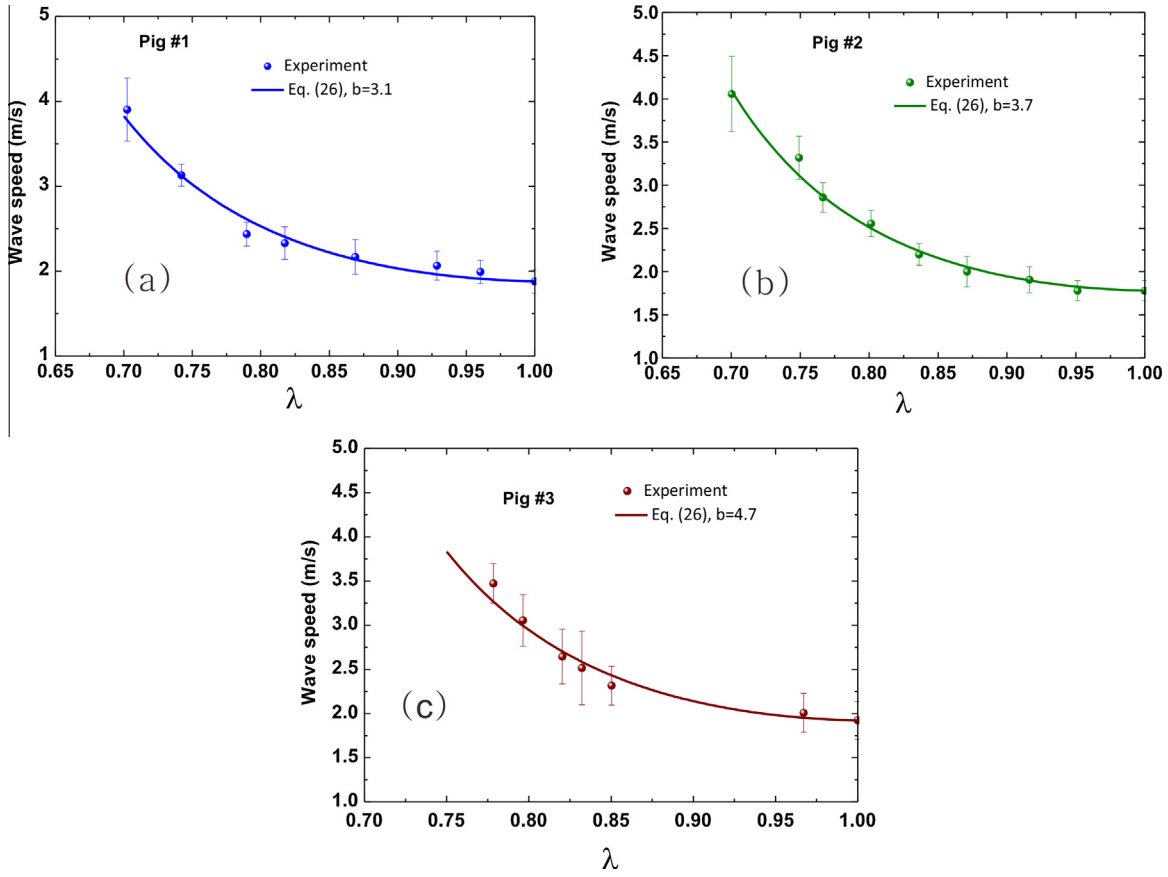


**Fig. 13.** Variations of the wave speeds with the stretch ratio  $\lambda$ . Points: experiments; solid lines: predictions using Eq. (26). (a) Pig #1; (b) Pig #2; and (c) Pig #3.

which nonlinear elastic deformation of the tissue affects the shear wave speed, which is used to evaluate the initial shear modulus  $\mu_0$  in the commercialized SSI method. Currently, the initial shear modulus  $\mu_0$  or elastic modulus has been adopted as a clinical indicator for disease diagnosis, e.g., for breast/thyroid tumor detection (Bercoff et al., 2004). Using the inverse approach developed in this

study, it is possible to evaluate the nonlinear elastic parameters besides the initial shear modulus using the SSI technique, e.g., the parameter  $b$ . The nonlinear elastic parameters may serve as novel clinical indicators because some diseases not only change the initial shear modulus of a soft tissue but also may alter its nonlinear elastic property.

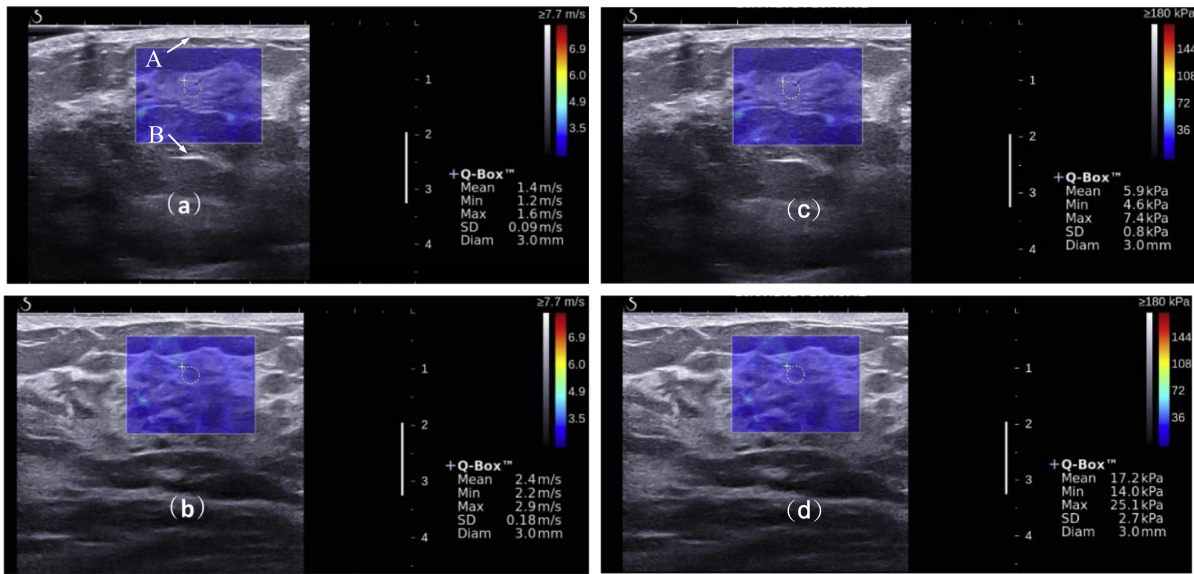


**Fig. 14.** Wave speeds and the elastic moduli in the region of interest (circled region in the figure). (a) wave speeds in the stress-free state; (b) wave speeds in the deformed state; (c) elastic moduli in the stress-free state; and (d) elastic moduli in the deformed state. The characteristic points A and B are used to determine  $\lambda$ ,  $\xi$  is about 0.1 according to the deformation in the horizontal direction.

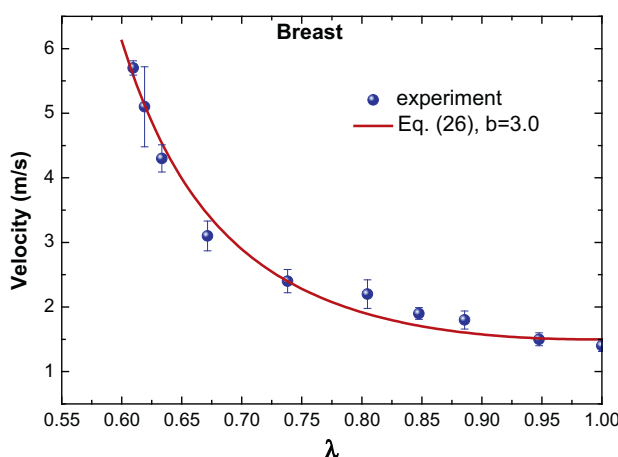


**Fig. 15.** Variation of the wave speeds in the glandular tissue of the breast with the stretch ratio  $\lambda$ .

## 6.2. Human heel fat pad

The human heel fat pad plays an important role in absorbing the shock and protecting against excessive local stress in everyday life. It is also believed that the mechanical behavior of the fat pad has a close relationship with the overuse injuries (Miller-Young et al., 2002). Besides, altered mechanical properties of the human heel pad have been implicated in the development of plantar heel pain. Therefore, the determination of the *in vivo* nonlinear elastic properties of the heel fat pad is not only an illustration of the usefulness of the proposed method but also has scientific and clinical significance. The two healthy male volunteers, 22 years old, and weigh 65 kg and 69 kg, respectively, participated in the experiments. The measurement was conducted by indenting the probe in the heel fat pad slowly (Fig. 16) and the shear wave speeds at different contact depths were recorded.

Fig. 17 shows the measured wave speeds at two different contact depths for the volunteer #2. The variations of the measured wave speed with the parameter  $\lambda$  are plotted in Fig. 18, which

together with the Eq. (27) permit to determine the parameter  $b$ . The initial shear moduli  $\mu_0$  for the two volunteers (#1 and #2) given by our measurements are 5.9 kPa and 5.4 kPa, respectively. The hyperelastic parameter  $b$  for volunteer #1 is  $b = 2.2 \pm 0.3$ , and  $b = 2.4 \pm 0.2$  for the volunteer #2. Miller-Young et al. (2002) have performed compression tests to characterize the *ex vivo* nonlinear elastic properties of the human heel fat pad. Fitting the stress-stretch ratio curves in their paper using the Demiray-Fung model, we obtain the parameter  $b$  varying from 0.7 to 1.7 depending on the loading speed. Our results are close to their value corresponding to the fast loading procedure. Weaver et al. (2005) measured the *in vivo* shear modulus of the human heel fat pads using magnetic resonance elastography (MRE). They did observe the increase in the measured shear modulus with the increasing compressive strain, but the nonlinear elastic parameters, e.g., the parameter  $b$  involved in this study, have not been quantitatively determined in their paper. To the authors' best knowledge, this study represents the first attempt to quantitatively determine the *in vivo* nonlinear elastic properties of the human soft tissues using the SSI technique. We have not found other *in vivo* results for the nonlinear elastic parameters of the human heel fat pad for comparison.

The nonlinear elastic property of the heel fat pad may depend on the gender, age and life habit, e.g., the type of shoes that one prefers to wear. Monitoring the variation of the nonlinear elastic parameter of the heel fat pad with the factors above using the



**Fig. 16.** The *in vivo* nonlinear elastic properties of the human heel fat pads are measured using the SSI technique and the method proposed in this study.

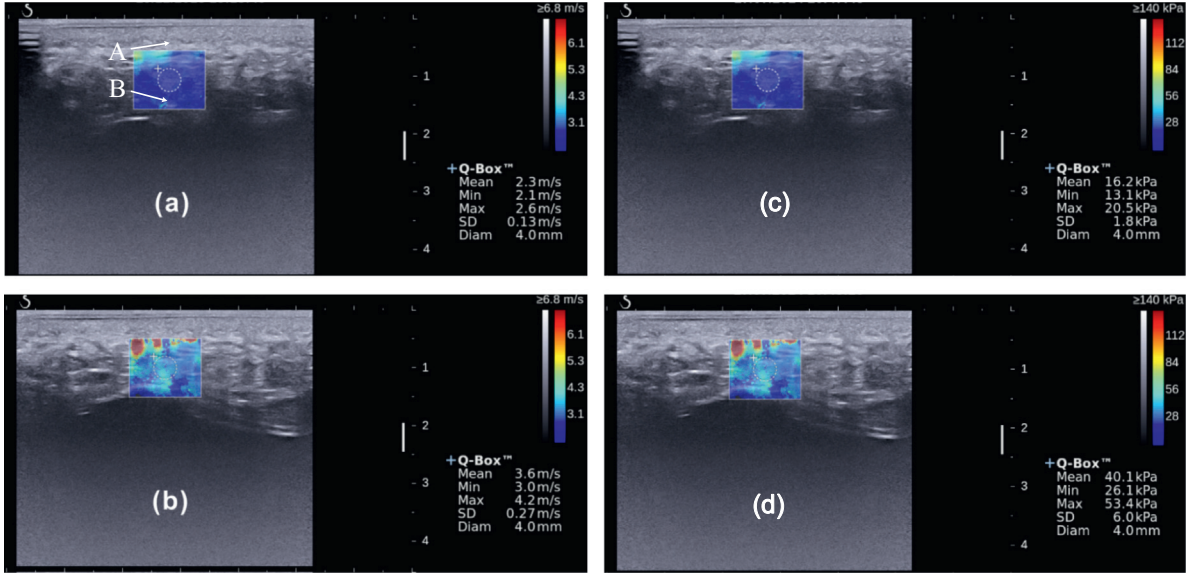


**Fig. 17.** Wave speeds and the elastic moduli in the region of interest (circled region in the figure) at two different indentation depths. (a) wave speeds in the stress-free state; (b) wave speeds in the deformed state; (c) elastic moduli in the stress-free state; and (d) elastic moduli in the deformed state. The characteristic points A and B are used to determine  $\lambda$ ,  $\xi$  is taken as 0.5 according to the deformation in the horizontal direction.

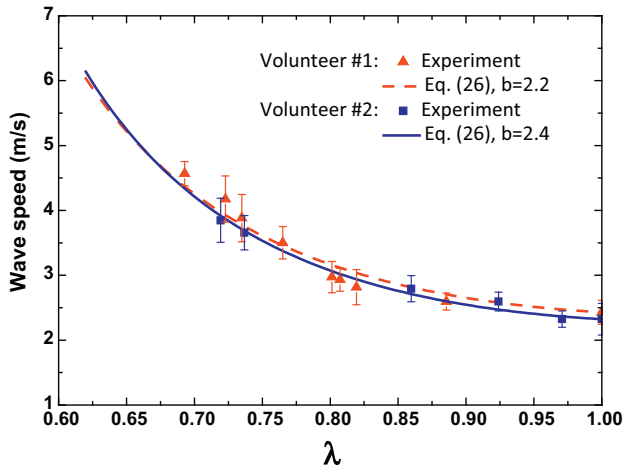


**Fig. 18.** Variations of the wave speeds with the stretch ratio  $\lambda$  for the two healthy volunteers, points represent the experimental results and lines are the predicted solutions using Eq. (26).

method proposed here may help understand their correlations with the overuse injuries or the development of plantar heel pain. This issue is interesting, for which the experiments are underway and the results may be reported in the coming future.

## 7. Generalization of the inverse analysis to other material models and limitations in this study

In this study, we focus on the hyperelastic soft tissue described via the constitutive model given by Eq. (24). It is emphasized that the general framework suggested here to develop an inverse approach can be easily applied to other material models. In order to illustrate this point, we take the Rivlin model (Destraete et al., 2011) as an example, for which the strain energy function is given by

$$W = C_{10}(I_1 - 3) + C_{01}(I_2 - 3) + C_{20}(I_1 - 3)^2, \quad (29)$$

where  $I_2 = \frac{1}{2}((\text{tr}(\mathbf{B}))^2 - \text{tr}(\mathbf{B}^2))$  and  $\mathbf{B} = \mathbf{F}\mathbf{F}^T$  is the left Cauchy-Green strain tensor.  $C_{10}$ ,  $C_{01}$  and  $C_{20}$  are material constants. The model

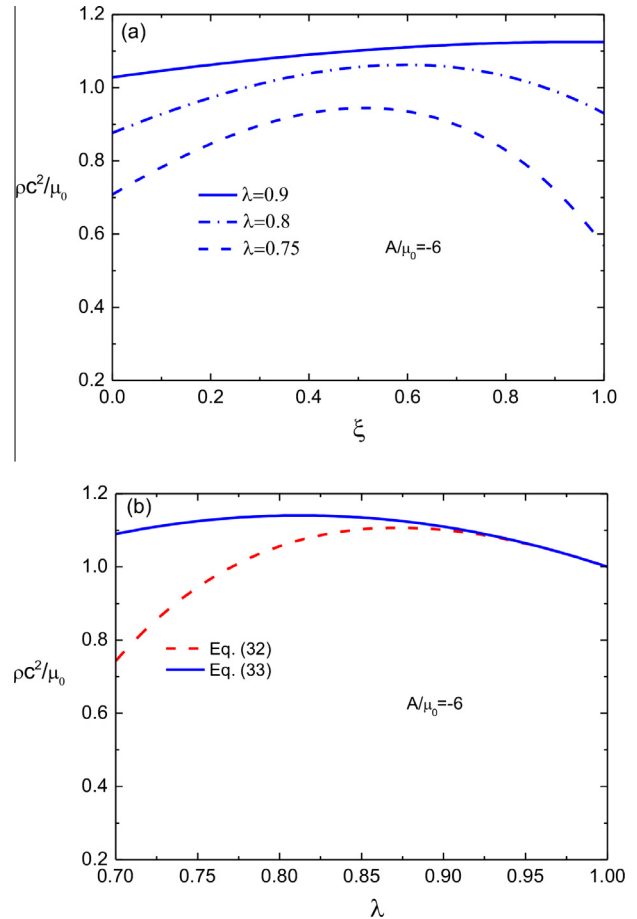


**Fig. 19.** (a) Dependence of the parameter  $\xi$  on the wave speed for different  $\lambda$ ; (b) a comparison of the solution given by Eq. (32) with that from Eq. (33), here  $\xi = 0.5$ .

given by Eq. (29) is equivalent to the fourth-order elastic model (Ogden, 1974; Hamilton et al., 2004) in the form of

$$W = \mu_0 \text{tr}(\mathbf{E}^2) + \frac{A}{3} \text{tr}(\mathbf{E}^3) + D(\text{tr}(\mathbf{E}^2))^2, \quad (30)$$

where  $\mathbf{E} = \frac{1}{2}(\mathbf{F}^T \mathbf{F} - \mathbf{I})$  is the Green strain tensor and  $\mathbf{I}$  a unit tensor. The material constants  $\mu_0$ ,  $A$  and  $D$  are related to  $C_{10}$ ,  $C_{01}$  and  $C_{20}$  by (Destrade et al., 2011)

$$\mu_0 = 2(C_{10} + C_{01}), A = -8(C_{10} + 2C_{01}), D = 2(C_{10} + 3C_{01} + 2C_{20}). \quad (31)$$

From Eqs. (30), (8) and (17) and for  $D = 0$ , we have

$$\begin{aligned} pc^2 &= (\lambda^{2-2\xi} + \lambda^{-4\xi} - \lambda^{-2\xi})\mu_0 \\ &+ \left( \frac{-5\lambda^{-2\xi}}{4} + \frac{\lambda^{-2}}{4} + \frac{\lambda^{2-2\xi} + \lambda^{-4\xi}}{2} \right)A. \end{aligned} \quad (32)$$

Fig. 19a illustrates the extent to which the parameter  $\xi$  affects the wave speed for different  $\lambda$ .

Note that the nominal strain  $e = \lambda - 1$ , under the condition of  $\xi = 0.5$  and  $\|e\| \ll 1$ , Eq. (32) reduces to

$$pc^2 = (1 + 2e^2)\mu_0 + \left( \frac{e}{4} + e^2 \right)A, \quad (33)$$

which is consistent with the solution adopted in the literature (Gennison et al., 2007; Latorre-Ossa et al., 2012). It should be pointed out that Eq. (33) is only valid for the case of  $\|e\| \ll 1$ , otherwise, Eq. (32) should be adopted. For the purpose of illustration, Fig. 19b compares the solution given by Eq. (32) with that given in Eq. (33) for the case of  $\xi = 0.5$ . It can be clearly seen that when  $\lambda < 0.85$ , Eq. (33) may contain significant errors.

In previous studies (Latorre-Ossa et al., 2012; Gennison et al., 2007), efforts have been made to determine the third order elastic constant  $A$  based on the model given by Eq. (30). Following the analysis performed in Section 3, we may evaluate the sensitivity

of the identified  $A$  to the errors in the measured wave speed  $c$  by defining the following condition number based on Eq. (32)

$$\Psi = \frac{c}{A} \frac{\Delta A}{\Delta c} = 2 + \frac{2A_0\mu_0}{A_1 A}, \quad (34)$$

where  $A_0 = (\lambda^{2-2\xi} + \lambda^{-4\xi} - \lambda^{-2\xi})$  and  $A_1 = \left( \frac{-5\lambda^{-2\xi}}{4} + \frac{\lambda^{-2}}{4} + \frac{\lambda^{2-2\xi} + \lambda^{-4\xi}}{2} \right)$ .

We plot the condition number given by Eq. (34) in Fig. 20 for different ratios of  $A/\mu_0$ .

Fig. 20 indicates that the sensitivity of the identified  $A$  to data errors depends on the loading condition. The greater the parameter  $\xi$  is, the more reliable the identified  $A$  will be, especially when  $\|A/\mu_0\| \leq 10$ . For a given loading condition, the smaller the parameter  $\lambda$  is, the more stable the identified solution will be. For example, for the case of  $\xi = 0.5$  and  $\|A/\mu_0\| \leq 10$ , the identified parameter  $A$  is not reliable when the input data corresponding to  $\|\lambda\| > 0.8$ , i.e.,  $\|e\| < 0.2$  are used. In this sense, the results in Fig. 20 may guide the practical experimental set-up, including the selection of appropriate loading conditions and loading range.

The limitations in this study are emphasized here, which may be useful for the users of our method. (i) Uniaxial loading condition adopted in previous studies is not required in our method, but we assume that the deformation in the region of interest is homogeneous and the loading direction is along one principal direction. (ii) The present analysis is limited to the case where the soft tissue is quasi-incompressible. (iii) In our analysis, the soft tissue is allowed to undergo finite deformation, i.e.,  $\lambda$  can be far from 1. However, the amplitude of the shear wave should be much smaller than the wavelength, so that the theory describing the propagation of the infinitesimal plane waves is applicable (Ogden, 2007). (iv) In this study, the soft tissue is assumed to be isotropic. When the soft

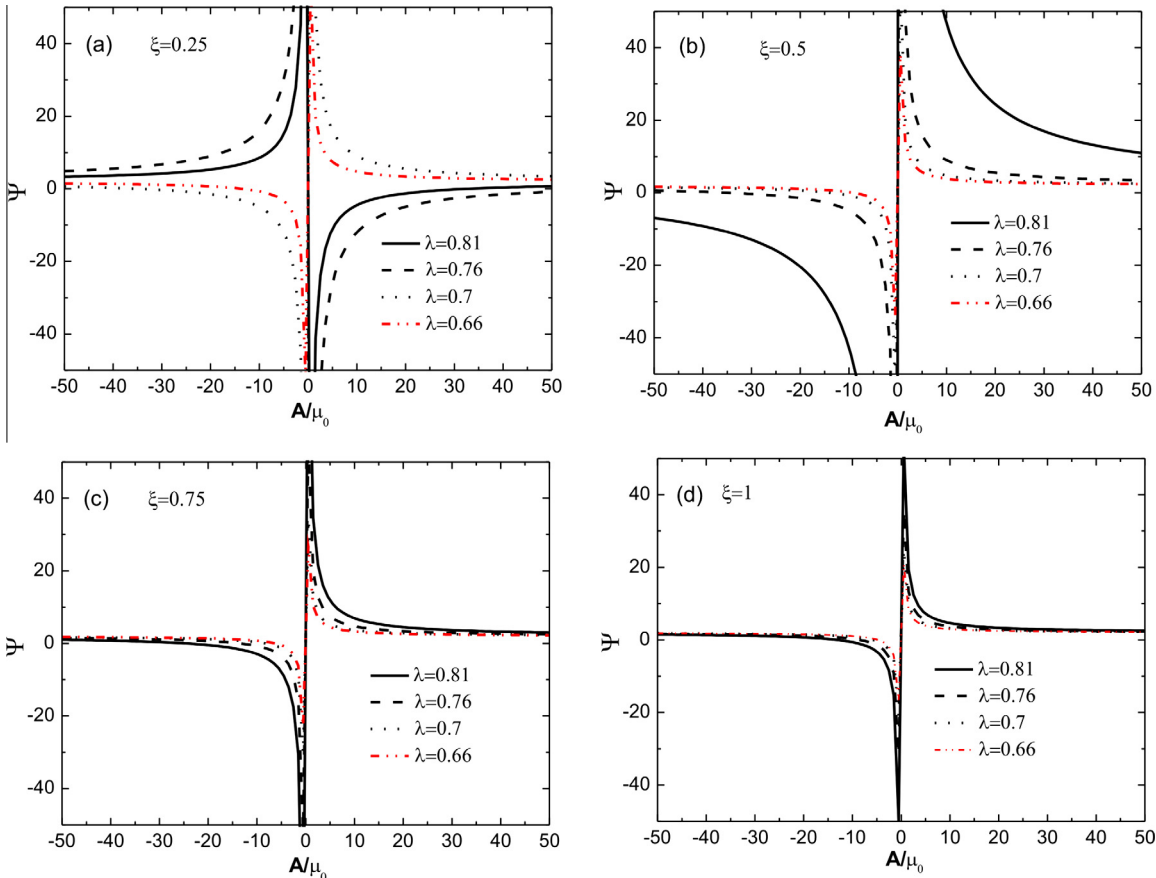


Fig. 20. Condition numbers for the determination of the parameter  $A$  using the data at different  $\lambda$  for the cases of (a)  $\xi = 0.25$ ; (b)  $\xi = 0.5$ ; (c)  $\xi = 0.75$ ; (d)  $\xi = 1$ .

tissue exhibits strong anisotropic deformation behavior, e.g., the deformation behavior of the muscle, the inverse method proposed here may be inapplicable. However, it is emphasized that the general solution given by Eq. (21) (Ogden, 2007) is applicable to the anisotropic hyperelastic materials. When the strain energy function for an anisotropic soft tissue is specified, the correlation among the wave speed, material properties and the deformation can be derived in analytical form. Furthermore, inverse approaches could be established to extract the material properties of the soft tissue from the experimental responses. However, when an anisotropic material model involves quite a few material parameters, the inverse problem is usually ill-posed or ill-conditioned and it would be a challenging issue to make clear the properties of the identified solution. (v) Finally, this study assumes that the soft tissue in the region of interest is homogeneous. As aforementioned a malignant tumor may have distinctly different elastic and/or nonlinear elastic properties from the soft tissue in around region. Therefore, evaluating the elastic and nonlinear elastic properties of the tumor may help differentiate whether it is malignant. However, it should be pointed out that a tumor is generally spatially non-homogeneous. In this sense, both the initial shear modulus and the nonlinear elastic parameter determined using the SSI technique and the inverse method proposed here can only be regarded as the equivalent elastic parameters of a tumor and their potential for clinical use requires further investigation.

## 8. Concluding remarks

The dynamic elastography has received considerable attention in clinical diagnosis in recent years. Continuum mechanics plays an essential role in understanding and developing this promising technique. This study is concerned with the nonlinear mechanics behind the supersonic shear imaging (SSI) technique which has been commercialized recently. Based on the current understanding on the propagation of plane shear wave in a stressed hyperelastic solid and the mathematical theory of inverse problems, we have suggested a general framework to develop inverse approaches to extract the nonlinear elastic properties from the experimental responses. In summary, the following key results have been obtained.

- Based on the elastodynamics theory, we have derived an analytical solution for the shear wave propagating in a stressed hyperelastic soft tissue described with the Demiray–Fung model. The result enables us to evaluate the extent to which the finite deformation affects the wave propagation when the material properties are given.
- Using the analytical solution derived here, we have proposed an inverse approach to extract the nonlinear elastic parameter of a soft tissue, i.e., the parameter  $b$  in the Demiray–Fung model. The properties of the solution to the inverse problem, i.e., the existence, uniqueness and stability of the solution have been investigated. The condition number measuring the sensitivity of the identified solution to data errors has been derived in closed-form, which could guide the experimental set-up.
- Numerical experiments have been carried out to validate the effectiveness of the novel inverse method. The results support our theoretical analysis on the properties of the solution to the inverse problem.
- Experiments on the phantom and *ex vivo* experiments on three pig livers were conducted to validate the inverse method. Both the initial shear modulus and the hyperelastic parameter  $b$ , which measures the nonlinear elastic deformation behavior of soft tissues, have been determined using the SSI technique and the proposed method. The results for the phantom are

basically consistent with those given by our tensile and indentation tests. The values for pig livers are reasonable in comparison with those reported in the literature (Roan and Vemaganti, 2007), demonstrating the applicability of the new method to practical measurements.

- *In vivo* experiments have been carried out to measure the elastic and nonlinear elastic properties of both the human breast tissue and the human heel fat pads. To the authors' best knowledge, this is the first time that the *in vivo* nonlinear elastic properties of the human soft tissues have been measured using the supersonic shear imaging technique. Our experiments demonstrate that the proposed method is suitable and convenient for *in vivo* measurements.
- In the proposed method, besides the stretch ratio  $\lambda$  in the loading direction, the parameter  $\xi$  is introduced to describe the deformation state. Therefore, the uniaxial loading condition adopted in previous studies (Latorre-Ossa et al., 2012; Gennisson et al., 2007) is not required here. To evaluate  $\lambda$  and  $\xi$ , the displacements at four characteristic points around the region of interest need to be recorded, which is not a difficult task in a commercialized ultrasound instrument. In this sense, our method can be easily implemented in the commercialized software, which deserves further efforts.
- Generalization of the proposed direct and inverse analysis to other material models is straightforward, which has been illustrated in this study by taking the Rivlin strain energy function as an example. This model has been used by other authors (Latorre-Ossa et al., 2012; Gennisson et al., 2007). Our results help understand the properties of the solution to the inverse problem, e.g., stability of the identified solution; therefore can provide useful information for practical measurements. The proposed inverse method allows one to determine the nonlinear elastic parameters of a soft tissue, which may serve as novel clinical indicators for the diagnosis of some diseases and monitoring their development. This issue has been briefly discussed in this study.

## Acknowledgements

Supports from the National Natural Science Foundation of China (Grant No. 11172155) and Tsinghua University – Beijing China (2012Z02103) are acknowledged. The authors acknowledge the help of Prof. Jianwen Luo and Mrs. Qiong He in the Medical School of Tsinghua University for preparing the phantom used in this study.

## References

- Bercoff, J., Tanter, M., Fink, M., 2004. Supersonic shear imaging: a new technique for soft tissue elasticity mapping. *IEEE Trans. Ultrasonics, Ferroelectr. Freq. Contr.* 51 (4), 396–409.
- Biot, M.A., 1940. The influence of initial stress on elastic waves. *J. Appl. Phys.* 11 (8), 522–530.
- Biot, M.A., 1965. *Mechanics of Incremental Deformations*. John Wiley and Sons, New York.
- Burnside, E.S., Hall, T.J., Sommer, A.M., et al., 2007. Differentiating benign from malignant solid breast masses with US strain imaging. *Radiology* 245 (2), 401–410.
- Chadwick, P., Ogden, R.W., 1971. A theorem of tensor calculus and its application to isotropic elasticity. *Arch. Ration. Mech. Anal.* 44 (1), 54–68.
- Chui, C., Kobayashi, E., Chen, X., Hisada, T., Sakuma, I., 2004. Combined compression and elongation experiments and non-linear modelling of liver tissue for surgical simulation. *Med. Biol. Eng. Comput.* 42, 787–798.
- Demiray, H., 1972. A note on the elasticity of soft biological tissues. *J. Biomech.* 5, 309–311.
- Destrade, M., Gilchrist, M.D., Saccomandi, G., 2010. Third- and fourth-order constants of incompressible soft solids and the acousto-elastic effect. *J. Acoust. Soc. Am.* 127, 2759–2763.

- Destrade, M., Goriely, A., Saccomandi, G., 2011. Scalar evolution equations for shear waves in incompressible solids: a simple derivation of the Z, ZK, KZK and KP equations. *Proc. Roy. Soc. A* 467 (2131), 1823–1834.
- Doyley, M.M., 2012. Model-based elastography: a survey of approaches to the inverse elasticity problem. *Phys. Med. Biol.* 57 (3), R35–R73.
- Foucher, J., Chanteloup, E., Vergniol, J., Castera, L., Le Bail, B., Adhoute, X., de Ledingen, V., 2006. Diagnosis of cirrhosis by transient elastography (FibroScan): a prospective study. *Gut* 55 (3), 403–408.
- Fung, Y.C., Fronek, K., Patitucci, P., 1979. Pseudoelasticity of arteries and the choice of its mathematical expression. *Am. J. Physiol.* 237 (5), H620–H631.
- Fung, Y.C., 1993. Biomechanics: Material Properties of Living Tissues. Springer.
- Gao, L., Parker, K.J., Lerner, R.M., Levinson, S.F., 1996. Imaging of the elastic properties of tissue—a review. *Ultrasound. Med. Biol.* 22 (8), 959–977.
- Gefen, A., Dilmoney, B., 2007. Mechanics of the normal woman's breast. *Tech. Health Care* 15, 259–271.
- Gennisson, J.L., Rénier, M., Catheline, S., Barrière, C., Bercoff, J., Tanter, M., Fink, M., 2007. Acoustoelasticity in soft solids: assessment of the nonlinear shear modulus with the acoustic radiation force. *J. Acoust. Soc. Am.* 122, 3211–3219.
- Gennisson, J.L., Deffieux, T., Macé, E., Montaldo, G., Fink, M., Tanter, M., 2010. Viscoelastic and anisotropic mechanical properties of *in vivo* muscle tissue assessed by supersonic shear imaging. *Ultrasound Med. Biol.* 36 (5), 789–801.
- Gokhale, N.H., Barbone, P.E., Oberai, A.A., 2008. Solution of the nonlinear elasticity imaging inverse problem: the compressible case. *Inverse Prob.* 24 (4), 045010.
- Hibbit, Karlsson and Sorensen Inc, USA, 2010. ABAQUS User and Theory Manual, Version 6.10.
- Hadamard, J., 1923. Lectures on the Cauchy Problem in Linear Partial Differential Equations. Yale University Press, New Haven, CT.
- Hamilton, M.F., Ilinskii, Y.A., Zabolotskaya, E.A., 2004. Separation of compressibility and shear deformation in the elastic energy density (L). *J. Acoust. Soc. Am.* 116, 41–44.
- Holzapfel, G.A., 2000. Nonlinear Solid Mechanics: A Continuum Approach for Engineering. John Wiley & Sons Ltd., England.
- Hussain, W., Ogden, R.W., 2001. The effect of pre-strain on the reflection and transmission of plane waves at an elastic interface. *Int. J. Eng. Sci.* 39 (8), 929–950.
- Itoh, A., Ueno, E., Tohno, E., et al., 2006. Breast disease: clinical application of US elastography for diagnosis. *Radiology* 239 (2), 341–350.
- Khaled, W., Ermert, H., 2008. Ultrasonic strain imaging and reconstructive elastography for biological tissue. In: Bioeng. Cell Tissue Res. Springer, Berlin Heidelberg, pp. 103–132.
- Krouskop, T.A., Dougherty, D.R., Vinson, F.S., 1987. A pulsed Doppler ultrasonic system for making noninvasive measurements of the mechanical properties of soft tissue. *J. Rehabil. Res. Dev.* 24 (2), 1–8.
- Latorre-Ossa, H., Gennisson, J., De Brosses, E., Tanter, M., 2012. Quantitative imaging of nonlinear shear modulus by combining static elastography and shear wave elastography. *IEEE Trans. Ultrasonics Ferroelectr. Freq. Contr.* 59 (4), 833–839.
- Mehrabian, H., Campbell, G., Samani, A., 2010. A constrained reconstruction technique of hyperelasticity parameters for breast cancer assessment. *Phys. Med. Biol.* 55 (24), 7489–7508.
- Miller-Young, J.E., Duncan, N.A., Baroud, G., 2002. Material properties of the human calcaneal fat pad in compression: experiment and theory. *J. Biomech.* 35 (12), 1523–1531.
- Miyanaga, N., Akaza, H., Yamakawa, M., Oikawa, T., Sekido, N., Hinotsu, S., Shiina, T., 2006. Tissue elasticity imaging for diagnosis of prostate cancer: a preliminary report. *Int. J. Urol.* 13 (12), 1514–1518.
- Ogden, R.W., 1974. On isotropic tensors and elastic moduli. *Mathematical Proceedings of the Cambridge Philosophical Society*, vol. 75. Cambridge University Press, pp. 427–436, No. 03.
- Ogden, R.W., 1997. Non-linear Elastic Deformations. Courier Dover Publications.
- Ogden, R.W., 2007. Incremental statics and dynamics of pre-stressed elastic materials. In: Waves in Nonlinear Pre-stressed Materials. Springer Vienna, pp. 1–26.
- Ophir, J., Cespedes, I., Ponnekanti, H., Yazdi, Y., Li, X., 1991. Elastography: a quantitative method for imaging the elasticity of biological tissues. *Ultrasonic Imag.* 13, 111–134.
- Ophir, J., Alam, S.K., Garra, B., Kallel, F., Konofagou, E., Krouskop, T., Varghese, T., 1999. Elastography: ultrasonic estimation and imaging of the elastic properties of tissues. *Proc. Inst. Mech. Eng. H: J. Eng. Med.* 213 (3), 203–233.
- Pavan, T.Z., Madsen, E.L., Frank, G.R., Jiang, J., Carneiro, A.A., Hall, T.J., 2012. A nonlinear elasticity phantom containing spherical inclusions. *Phys. Med. Biol.* 57 (15), 4787–4804.
- Rifai, K., Cornberg, J., Mederacke, I., Bahr, M.J., Wedemeyer, H., Malinski, P., Gebel, M., 2011. Clinical feasibility of liver elastography by acoustic radiation force impulse imaging (ARFI). *Dig. Liver Dis.* 43 (6), 491–497.
- Roan, E., Vemantti, K., 2007. The nonlinear material properties of liver tissue determined from no-slip uniaxial compression experiments. *J. Biomech. Eng.*, 450–456.
- Sandrin, L., Tanter, M., Catheline, S., Fink, M., 2002a. Shear modulus imaging with 2-D transient elastography. *IEEE Trans. Ultrasonics Ferroelectr. Freq. Contr.* 49 (4), 426–435.
- Sandrin, L., Tanter, M., Gennisson, J.L., Catheline, S., Fink, M., 2002b. Shear elasticity probe for soft tissues with 1-D transient elastography. *IEEE Trans. Ultrasonics Ferroelectr. Freq. Contr.* 49 (4), 436–446.
- Sarvazyan, A., Hall, T.J., Urban, M.W., Fatemi, M., Aglyamov, S.R., Garra, B.S., 2011. An overview of elastography – an emerging branch of medical imaging. *Curr. Med. Imag. Rev.* 7 (4), 255–282.
- Sarvazyan, A.P., Urban, M.W., Greenleaf, J.F., 2013. Acoustic waves in medical imaging and diagnostics. *Ultrasound Med. Biol.* 39, 1133–1146.
- Schaar, J.A., de Korte, C.L., Mastik, F., Strijder, C., Pasterkamp, G., Boersma, E., van der Steen, A.F., 2003. Characterizing vulnerable plaque features with intravascular elastography. *Circulation* 108 (21), 2636–2641.
- Thitaikumar, A., Krouskop, T.A., Garra, B.S., Ophir, J., 2007. Visualization of bonding at an inclusion boundary using axial-shear strain elastography: a feasibility study. *Phys. Med. Biol.* 52 (9), 2615–2633.
- Thitaikumar, A., Mobbs, L.M., Kraemer-Chant, C.M., Garra, B.S., Ophir, J., 2008. Breast tumor classification using axial shear strain elastography: a feasibility study. *Phys. Med. Biol.* 53, 4809–4823.
- Timoshenko, S., Goodier, J.N., 1951. Theory of Elasticity. McGraw-Hill Book Company.
- Weaver, J.B., Doyley, M., Cheung, Y., Kennedy, F., Madsen, E.L., Van Houten, E.E., Paulsen, K., 2005. Imaging the shear modulus of the heel fat pads. *Clin. Biomed.* 20, 312–319.
- Xu, H., Varghese, T., Madsen, E.L., 2011. Analysis of shear strain imaging for classifying breast masses: finite element and phantom results. *Med. Phys.* 38, 6119–6127.
- Zhang, M.G., Cao, Y.P., Li, G.Y., Feng, X.Q., 2014. Pipette aspiration of hyperelastic soft materials: Theoretical analysis, simulations and experiments. *J. Mech. Phys. Solids* 68, 179–196.